# On the Total, Mean, and Eddy Heat and Freshwater Transports in the Southern Hemisphere of a 1/8° × 1/8° Global Ocean Model

A. J. MEIJERS

*Antarctic Climate and Ecosystems Cooperative Research Centre and Institute of Antarctic and Southern Ocean Studies, University of Tasmania, and CSIRO Marine Research, Hobart, Tasmania, Australia*

N. L. BINDOFF

*Antarctic Climate and Ecosystems Cooperative Research Centre, Tasmanian Partnership for Advanced Computing, and Institute of Antarctic and Southern Ocean Studies, University of Tasmania, and CSIRO Marine Research, Hobart, Tasmania, Australia*

J. L. ROBERTS

*Antarctic Climate and Ecosystems Cooperative Research Centre and Tasmanian Partnership for Advanced Computing, University of Tasmania, Hobart, Tasmania, Australia*

(Manuscript received 17 November 2005, in final form 22 May 2006)

ABSTRACT

The large-scale volume, heat, and freshwater ocean transports in the Southern Hemisphere are investigated using time-averaged output from a seasonless, high-resolution general circulation model. The ocean circulation is realistic, and property transports are comparable to observations. The Antarctic Circumpolar Current (ACC) carries 144 Sv (Sv $\equiv 10^6$ m$^3$ s$^{-1}$) of water eastward across Drake Passage, increasing to 155 Sv south of Australia because of the Indonesian Throughflow (ITF). There is a clear Indo-Pacific gyre around Australia exchanging −10 Sv, 0.9 PW of heat, and 0.2 Sv of freshwater through the ITF, and there is a 9-Sv leakage from the Tasman Sea to the Indian Ocean. The transport of heat and freshwater by eddies is localized to the upper 1000 m of the water column and specific regions, such as western boundary currents, confluences, and the subantarctic front (SAF). Eddy transport of heat and freshwater is negligible in gyre interiors and south of the SAF but is vital across the northern edge of the ACC, in particular at the Agulhas Retroflection where eddies accomplish almost 100% of the net ocean heat and 60% of the southward freshwater transport. The eddy transport is almost zero across the latitude of Drake Passage while in a quasi-Lagrangian frame eddy transports are significant across the ACC but surprisingly are still smaller than the mean transport of heat. Mean and eddy property transport divergences are found to be strongly compensating in areas of high eddy activity. This is caused by increased baroclinic instability in strong mean flows, which induces an opposing eddy transport. This relationship is observed to be stronger in the case of horizontal heat transport than in corresponding horizontal freshwater transports.

## 1. Introduction

Mesoscale eddies play an important role in the oceanic transport of heat and freshwater, in addition to the main thermohaline and upper-ocean circulations. Sea surface height measurements indicate that eddies are ubiquitous over the global ocean, although they are more active in regions of strong, narrow flow and current confluences, such as western boundary currents and the Antarctic Circumpolar Current (ACC) (Rhines 2001). The difficulties inherent in gathering and observing the transport by these small-scale (both spatial and temporal) features means that eddy transports are one of the most underobserved oceanographic properties. Wunsch's (1999) global compilation of observational studies finds that zonally integrated eddy transports are generally small, but can be significant on small spatial scales. Regions of particular significance include the western boundary currents, the Tropics, and the ACC. These regions are consistent with Stammer's (1998)

*Corresponding author address:* Andrew Meijers, IASOS, University of Tasmania, Private Bag, 7001 Tasmania, Australia.
E-mail: ameijers@utas.edu.au

DOI: 10.1175/JPO3012.1

Ocean Topography Experiment (TOPEX)/Poseidon altimetry data analysis.

Property transport by eddy activity appears to be particularly important across the ACC where there can be no mean geostrophic flow across mass transport streamlines (De Szoeke and Levine 1981). The ocean loses a substantial amount of heat to the atmosphere south of the ACC, however, requiring a poleward heat flux. A current meter study south of Australia by Phillips and Rintoul (2000) found that the 0.9 PW of heat transported poleward by eddy activity (extrapolating along the full length of the ACC) is sufficient to accomplish the required meridional transport. The importance of this cross-ACC eddy transport is noted by De Szoeke and Levine (1981), Sloyan and Rintoul (2001), and Olbers and Visbeck (2005), but several aspects remain unresolved, including the spatial distribution, depth range, and degree of significance outside the ACC.

Recent use of quasi-Lagrangian coordinates has assisted in understanding the dynamics of momentum and heat transport across the zonally unconstrained Drake Passage. When zonally averaged on isopycnal coordinates the large cross-isopycnal flux implied by the Deacon cell vanishes (Döös and Webb 1994) as the mean transport overturning is balanced by an opposing eddy transport. This compensation leads to a residual-mean transport in quasi-Lagrangian coordinates where southward heat transport by mean eddy-driven cells in the meridional plane largely balances the mean Eulerian Deacon cell, with the small residual representing the net heat transport. Studies utilizing such approximations to the Lagrangian mean find that eddies appear as the primary means for the transport of heat southward across the ACC (Marshall and Radko 2003; Olbers and Visbeck 2005).

The paucity of observational data means that studies have been largely limited to high-resolution eddy-resolving numerical models. One interesting result from these studies is that the net meridional heat transport is insensitive to model resolution, ranging from inverse models (Ganachaud and Wunsch 2000; Sloyan and Rintoul 2001; Ganachaud 2003), through non-eddy-resolving climatological models (Stammer et al. 2003), to high-resolution eddy-resolving models (McCann et al. 1994, and the current study). Conversely, Beckmann et al. (1994) found that increasing model resolution results in greater eddy transports. This influence of resolution was also observed by Jayne and Marotzke (2002) who noted an increased eddy heat transport in a ¼° resolution run of the Parallel Ocean Climate Model (POCM) over a previous ½° experiment by Semtner and Chervin (1992). Drijfhout (1994) proposed that the cause of this relationship is due to regions of mean flow convergence or divergence inducing eddy transport via increased horizontal thermal gradients that redistribute heat downgradient and thus oppose the mean flow. As this often occurs over small scales, increased model resolution results in increased mean transport/flux and, hence, induces a corresponding increase in the compensating eddy heat transport/flux. An increased understanding of the eddy dynamics is therefore important for the effective parameterization of these subgrid-scale effects in low-resolution coupled climate models, which currently may misrepresent important ocean processes (Willebrand and Haidvogel 2001).

There is a scarcity of literature on the transport of freshwater by eddies, but results from McCann et al. (1994) and Stammer (1998) indicate that significant freshwater transports also occur in similar regions to heat transports. The net eddy freshwater transport across the ACC is northward, as the Southern Ocean is a significant ($\approx$0.5 Sv; Sv $\equiv 10^6$ m$^3$ s$^{-1}$) freshwater source south of 30°S (Wijffels et al. 1992). There is relatively more freshwater transport at depth, when compared with heat transport, and this is likely to result in a reduced eddy contribution to the total freshwater transport, as significant eddy transport is largely restricted to the upper-ocean layers.

An analysis of eddy heat and freshwater transport in the Southern Hemisphere of a high-resolution global ocean model is the focus of this study. A description of the numerical model used is presented in section 2. The modeled horizontal and meridional mean volume transport streamfunctions are presented in section 3, along with a summary of important heat and freshwater transports. These indicate that the model largely replicates the known ocean circulation. Sections 4 and 5 consider the mean and eddy transports of heat and freshwater, respectively. The eddy and mean transports are examined by basin and depth interval, primarily highlighting the importance of the upper ocean around the subantarctic front (SAF) and boundary currents. The divergence of these fields and the pointwise mean and eddy contributions to the total flux are also examined. Section 6 discusses these results and draws conclusions.

## 2. Model description and methods

The dataset used in this analysis was created using the Tasmanian Partnership for Advanced Computing (TPAC) ⅛° ocean model with constant wintertime forcing. This is a primitive equation, ocean-only general circulation model based on the Geophysical Fluid Dynamics Laboratory's Modular Ocean Model (MOM),

version 3.0. The model domain extends from 80°S to 80°N with a ⅛° resolution in both horizontal directions, and has 24 depth levels with partial bottom cells to produce realistic bottom topography.

The model was integrated for 20 yr, using asynchronous time stepping (6 min for velocities and 30 min for tracers). Velocities were initialized to zero, and initial temperatures and salinities were taken from the World Ocean Circulation Experiment (WOCE) Hydrographic Programme–Special Analysis Centre (WHP–SAC) atlas (Gouretski and Janke 1998) supplemented by Levitus (1982) data in the Arctic Ocean. Restoring boundary conditions loosely constrain the sea surface temperature and salinity (SST and SSS) to fixed reference values of hemispheric wintertime conditions (blended across the equator) with a Newtonian restoring time scale of 30 days. These seasonless boundary conditions reduced the distorted physics associated with the asynchronous time-stepping regime and should agree with a synchronous integration when in a steady state. Momentum fluxes were calculated using the yearly wind stress average taken from National Centers for Environmental Prediction–National Center for Atmospheric Research (NCEP–NCAR) reanalysis data (Kalnay et al. 1996).

This model is unusual, being both eddy resolving and including isoneutral mixing in the form of Gent and McWilliams (1990) subgrid-scale mixing, as was also used in Roberts and Marshall (1998) and Smith and Gent (2004). This subgrid-scale mixing along with the seasonless nature of the model was chosen to emphasize the role of mesoscale dynamics in larger-scale ocean dynamics and to eliminate boundary condition variability. The 20-yr integration period with high spatial and temporal resolution provides sufficient data for statistical relationships such as mean flow and eddy properties to be calculated. Model flux drift, represented by the increased storage of heat and salt, is insignificant when compared with the horizontal and freshwater transports for this study.

All velocity, tracer transport values, and eddy statistics for heat and freshwater used in this study were accumulated for every time step and stored annually. These annual accumulations were averaged to form the annual mean statistics of model years 10–20 described below. This period was chosen to avoid any model instabilities and drift in the early years of the simulation, and is long enough to provide stable estimates of the transports. The salinity anomaly $S$ used in this study is calculated as $S = (S' - S_0)/S_0$, where $S'$ is the actual ocean salinity (psu) and $S_0$ is a reference salinity of 35 psu. The freshwater flux anomaly, referred to as freshwater transport in this paper, is therefore the negative of the salinity anomaly. The term heat transport is also used when referring to the potential temperature transport relative to 0°C.

The total property transports used in this study were decomposed into the sum of a mean and an eddy component, so for the heat transport

$$\overline{v\theta} = \overline{v}\,\overline{\theta} + \overline{v'\theta'}. \tag{1}$$

Here, an overbar denotes the time mean and a prime denotes the deviation from the time mean. Following Jayne and Marotzke (2002), the potential temperature transports in Eq. (1) were scaled by the specific heat content and the average density of seawater to give the heat transport, and the "eddy transport" term actually includes all variability from the mean on all temporal and spatial scales, not just mesoscale perturbations.

The mean heat transport is further decomposed in Eq. (2), such that the total heat transport is described as the sum of a mean vertical (or overturning) component (first component on right-hand side), mean horizontal (or gyre) components (middle three on right-hand side), and the eddy component (final component on right-hand side):

$$\overline{V\theta} = \langle\overline{V}\rangle\langle\overline{\theta}\rangle + \langle\overline{V}\rangle\overline{\theta^*} + \overline{V^*}\langle\overline{\theta}\rangle + \overline{V^*}\,\overline{\theta^*} + \overline{V'\theta'}. \tag{2}$$

Here, $\langle\,\rangle$ denotes the zonal mean, and an asterisk indicates the deviation from this horizontal mean. This decomposition was similarly performed for freshwater transport.

This decomposition in an Eulerian coordinate system is not always appropriate, particularly across Drake Passage (Döös and Webb 1994). Bryan (1986) noted that mean eddy-driven cells in the meridional plane act to compensate for the eddy term in Eq. (1), consequently leading to an underestimation of the eddy transport in some situations. More recent theoretical advances have used techniques such as the transformed Eulerian mean (McIntosh and McDougall 1996; Marshall and Radko 2003) or a quasi-Lagrangian isopycnal framework (Marshall 1997) to more accurately describe the eddy flux across fronts, particularly the ACC, and such frameworks account for the tendency for eddies to transport properties along isopycnals (Olbers and Visbeck 2005). This analysis, however, remains within the natural $z$ coordinates of the model in the Eularian frame in order to simplify analysis and compare the results with similar analyses. A quasi-Lagrangian framework along mass transport streamlines in place of lines of constant latitude is adopted for analysis of the property transport across the ACC to determine the importance of eddies in the region.

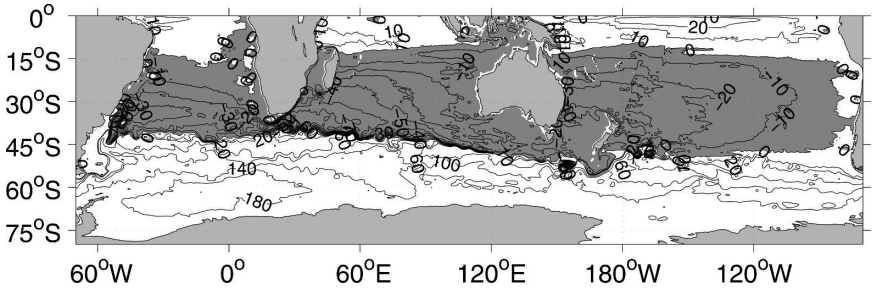


FIG. 1. Depth-integrated mass transport streamfunction (Sv). Positive values indicate clockwise volume transport parallel to streamlines and negative (shaded) values indicate counterclockwise volume transport.

## 3. General ocean circulation

### *a. Horizontal circulation*

The calculated volume transport streamfunction is shown as a function of latitude and longitude in Fig. 1 and as a function of latitude and depth in Fig. 2. These volume transports were calculated in the manner of Döös and Webb (1994) such that

$$\psi_h(x, y) = \int_0^x \int_{\text{bottom}}^0 v(x, y, z)\, dz\, dx, \qquad (3)$$

where $\psi_h(x, y)$ is the horizontal streamfunction as a function of latitude ($y$) and longitude ($x$). Here, $v$ is the northward velocity defined at $x$, $y$, and depth ($z$). The meridional streamfunction $\psi_m(y, z)$ is similar, but integrated first zonally and then by depth.

The horizontal, depth-integrated volume transport displays a well-defined ACC; subtropical, tropical, and polar gyres; and strong western boundary currents. The ACC in particular displays clear mesoscale features, despite time averaging, due to either standing eddies or topographical influences and indicates their relative temporal invariance. This supports Karoly et al. (1997) in that standing eddies are the major contributors to zonal spatial variability.

Meridional sections at "chokepoints" of the ACC (Table 1) indicate that 144 Sv of water is transported eastward across Drake Passage, increasing to 145 Sv between Africa and Antarctica. The addition of south Indian Ocean water increases this to 155 Sv between Australia and Antarctica. The additional volume represents the Indonesian Throughflow (ITF). These values agree with other observations of the ACC strength (Rintoul and Sokolov 2001; Sloyan and Rintoul 2001; Whitworth and Peterson 1985; Yaremchuck et al. 2001), although they may be biased toward larger values because of the perpetual wintertime forcing used in this model. Table 1 also gives the heat and freshwater transports through these chokepoints. Across Drake Passage, 1.4 PW of heat are transported eastward, decreasing to 1.2 PW between Antarctica and Africa at 20°E. These transports are slightly higher than Ganachaud and Wunsch's (2000) WOCE-based inverse model predictions of 1.3 and 0.9 PW, and Stammer et al.'s. (2003) 1.14 ± 0.06 and 1.01 ± 0.15 PW from a 2° OGCM. The ACC's zonal heat transport increases to around 2 PW south of Australia because of the addition of heat from the Indian Ocean. This value is consistent with Yaremchuck et al.'s (2001) observed transport of 1.82 ± 0.53 PW between Antarctica and Tasmania. Eastward freshwater transport in the Southern Ocean reduces from 2.3 Sv at 67°W to 2.2 Sv south of Africa and further to 2.1 Sv at 118°E. South of Australia, however, there is a net equivalent precipitation of 0.1 Sv, increasing the eastward transport to 2.2 Sv at 146°E.

There is a westward-flowing boundary current against the Antarctic continent south of the Antarctic slope front (ASF), particularly in the presence of the Ross and Weddell Sea gyres, where flow approaches 60 Sv. These gyres are possibly overestimated in this study, in comparison with Semtner and Chervin's (1992) record of around 30 Sv, because of the lack of sea ice in the model and winter wind bias. The 29.4 ± 14.7 Sv Antarctic coastal recirculation gyre noted by Bindoff et al. (2000) at around 100°E carries around 10–15 Sv in this model, and is in the range of the uncertainties associated with these observations. The anticyclonic recirculation gyre immediately south of Tasmania (Rintoul and Sokolov 2001; Yaremchuck et al. 2001) is also present, although at 16 Sv it is not as strong as the observed 22 Sv. Approximately 9 Sv of this flow is transported from the Tasman Sea through the weak anticyclonic gyre in the Great Australian Bight into the Indian Ocean and possibly represents the Tasman leakage described by Gordon (2001) and Speich et al. (2002). This leakage carries 0.5 PW westward at 118°E.

The Brazil Current transports approximately 35 Sv of water southward to 40°–50°S where it meets the Malvi-

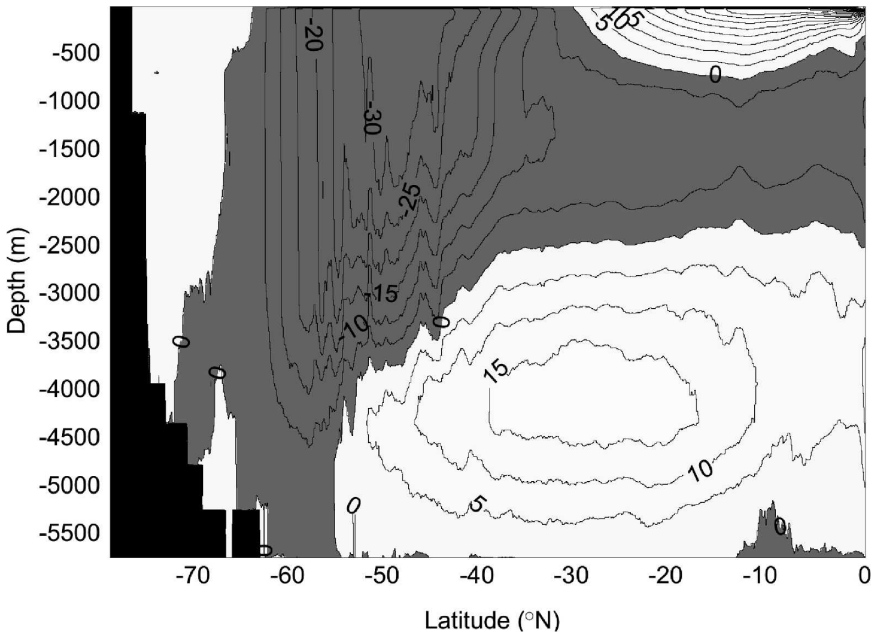


FIG. 2. Zonally integrated meridional mass transport streamfunction (Sv). Positive values indicate counterclockwise volume transport parallel to streamlines and negative (shaded) values indicate clockwise volume transport.

nas Current, which transports 110 Sv at 50°S. The 50 Sv carried north at the confluence correlates well with the 45 ± 7 Sv observed by Maamaatuaiahutapu et al. (1998). The equatorward-flowing Benguela Current is fed by 10 Sv of Agulhas leakage, and transfers 0.4 PW westward into the Atlantic Ocean. This in turn feeds the North Brazil Current system and hence represents the "warm" return pathway for the North Atlantic Deep Water (NADW). This supports the 0.3 PW reported by Gordon et al. (1992). The net southward Atlantic transport is slightly less than 1 Sv (Table 2), consistent with the small Bering Straight throughflow.

The Agulhas Current transports more than 70 Sv of water southward at 37°S, in agreement with the observations by Stramma and Lutjeharms (1997). The Mozambique Channel carries 17 Sv of this flow, 10 Sv of which stems from the Indonesian Throughflow, while the remainder comes from the recirculation of the Indian Ocean gyre. This compares extremely well to the values presented in Biastoch and Krauss (1999) and Stammer et al.'s. (2003) WOCE-constrained model results. The net 10-Sv southward transport due to the ITF is consistent with Sloyan and Rintoul's (2001) estimate of 10.4 ± 3.1 Sv. The ITF also carries 0.9 PW into the Indian Ocean basin. This value is slightly smaller than estimates reported in Stammer et al. (2003) (1.12 ± 0.59 PW), Ganachaud and Wunsch (2000) (1.4 PW), and Ganachaud and Wunsch (2003) (>1 PW). The ITF freshwater transport is 0.2 Sv into the Indian Ocean and is supported by Ganachaud and Wunsch (2003) and Wijffels (2001), who suggest a value of 0.2 Sv but warn that this is a poorly understood quantity.

TABLE 1. Zonal "chokepoint" mass heat and freshwater transports; positive is eastward.

| | Lon | Volume (Sv) | Heat (PW) | Freshwater (Sv) |
|---|---|---|---|---|
| Southern Ocean | 67°W | 144 | 1.4 | 2.3 |
| | 20°E | 145 | 1.2 | 2.2 |
| | 115°E | 155 | 2.1 | 2.1 |
| | 146°E | 155 | 1.9 | 2.3 |
| ITF | 115°E | −10 | −0.9 | −0.2 |

TABLE 2. Meridional mass heat and freshwater transports by basin; positive is northward.

| | Lat (°S) | Volume (Sv) | Heat (PW) | Freshwater (Sv) |
|---|---|---|---|---|
| Pacific | 18 | 11 | −0.9 | 0.2 |
| | 32 | 11 | 0.9 | 0.3 |
| Indian | 20 | −10 | −1.2 | −0.2 |
| | 32 | −10 | −1 | 0.2 |
| Atlantic | 30 | −1 | 0.3 | 0.2 |
| | 19 | −1 | 0.3 | 0.1 |
| | 11 | −1 | 0.3 | −0.1 |
| | 5 | −1 | 0.4 | −0.2 |

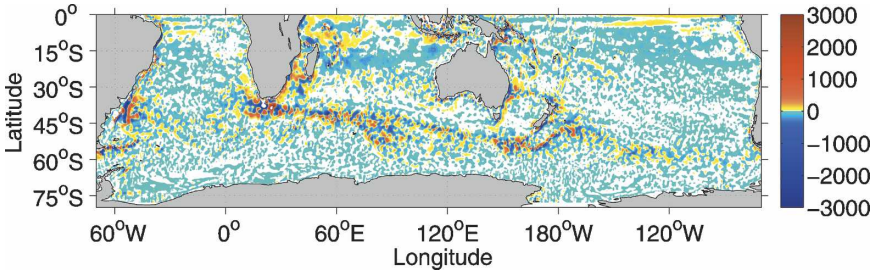


FIG. 3. Depth-integrated eddy heat convergence (W $m^{-2}$). Negative values represent heat divergence. Note the compressed color scale indicating the insignificance of eddy transport across much of the ocean.

The Pacific Ocean exhibits two depth-integrated gyre systems; the large subtropical gyre transporting almost 40 Sv around the basin from 45° to 15°S, and the smaller (30 Sv) equatorial gyre. The subtropical gyre exhibits a northward internal flow over the majority of the basin and has a fairly modest return flow in the East Australian Current (EAC), which increases in strength from 10 Sv at 20°S to 20–30 Sv at 30°S; the variation being due to the retroflection of the current noted by Mata et al. (2000), who measured the mean southward flow as 22.1 ± 4.6 Sv. Around 20 Sv travels zonally across the north of the Tasman Sea to feed the east Auckland boundary current while 9 Sv moves south past Tasmania as a leakage current from the Pacific to Indian Oceans. The net northward transport of 11 Sv over the Pacific basin closes the global volume transport and is in close agreement with McCann et al. (1994), Ganachaud and Wunsch (2000), and Sloyan and Rintoul (2001).

### *b. Meridional circulation*

Four distinct meridional cells are apparent in the Eulerian zonally integrated meridional mass transport streamfunction (Fig. 2). We label them the Deacon, subpolar, deep, and subtropical cells (Döös and Webb 1994). The Deacon cell extends from 35° to 60°S and from the surface to a depth of 3500 m. Here, the prevailing westerly winds drive an equatorward Ekman layer, extending from south of the polar front to about 32°S and transporting more than 30 Sv (at 50°S) of low-salinity, cold water northward. This agrees well with other studies (Semtner and Chervin 1992; Döös and Webb 1994; Jayne and Marotzke 2001; Sloyan and Rintoul 2001). Between 50°S and the convergence with the southward subtropical gyre transport at 30°S, more than 20 Sv of the Ekman layer is subducted, returning southward at a depth of between 1000 and 3500 m and closing this circulation north of Drake Passage (≈60°S). At 35°S the remainder of the Ekman layer (10 Sv) is subducted beneath the warmer, more saline subtropical cell, forming low-salinity Subantarctic Mode Water (SAMW) and traveling toward the equator at a depth of between 700 and 1200 m.

The intermediate-depth northward flow is partially balanced by the return flow of Circumpolar Deep Water (CDW) moving southward between 1600 and 2200 m, below a largely quiescent zone at 1500 m, roughly corresponding to the low-salinity tongue and also the ocean oxygen minimum. This water mass (10 Sv) forms the subpolar cell that moves beneath the Deacon cell and eventually upwells at around 65°S. The outcropping leads to around 10 Sv of deep water being converted into intermediate and upper water through atmospheric interaction (Döös and Coward 1997).

The large deep cell that extends from around 3000 m to the ocean floor and from 55°S to north of the equator circulates approximately 18 Sv. It is worth noting that the zero contour separates the deep cell from the global ocean south of 55°S. The model therefore does not accurately represent the northward spreading of Antarctic Bottom Water (AABW) and probably results from the lack of explicit sea ice formation in bottom water formation areas. The net deep southward transport is consistent with the subsequent upwelling south of the polar front (≈10 Sv) required to balance the sinking of NADW and close the global overturning cell (Rintoul et al. 2001).

## 4. Eddy heat transport

### *a. Horizontal eddy heat transport*

The depth-integrated eddy heat divergence (Fig. 3) identifies regions of significant eddy heat transport activity. The boundary currents and confluences, particularly the Agulhas Retroflection, are areas of high eddy activity, while the subtropical gyre interiors are relatively devoid of perturbations from the mean flow. The ACC in general, and the southwest Indian Ocean SAF sector in particular, are important regions of eddy heat transport.

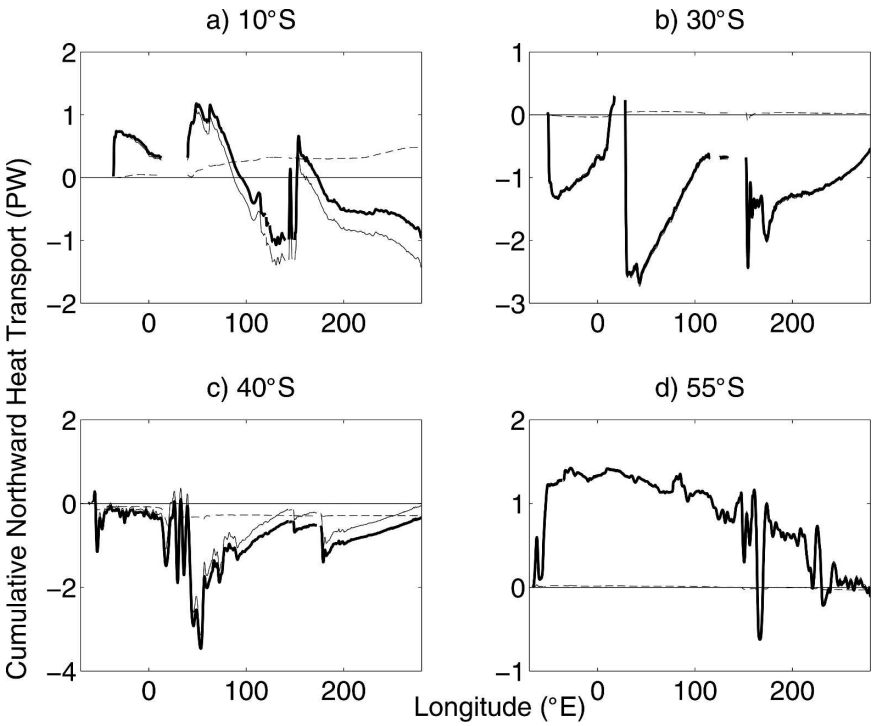


FIG. 4. Cumulatively summed (east–west) total (thick line), mean (thin), and eddy (dashed) meridional heat transports at (a) 10°, (b) 30°, (c) 40°, and (d) 55°S (PW). Positive slopes indicate northward heat transport.

The strong correlation between the mean and total heat transports, particularly in the subtropics and south of the SAF (Figs. 4b and 4d), indicates that the meridional transport of heat is primarily accomplished by the mean ocean flow on a point-by-point basis and that mesoscale eddy activity is restricted to energetic regions of volume transport (Spall and Chapman 1998). For example, the Agulhas Retroflection eddy component achieves almost 0.3 PW of southward heat transport at 40°S, and to a lesser extent the Brazil Current and EAC also have significant eddy components.

The vertical and horizontal mean and the eddy components of northward heat transport [Eq. (2)] can be considered on an individual ocean basin basis (Fig. 5). The South Atlantic Ocean generally exhibits a small (<0.05 PW) northward eddy heat transport while in the Indian and Pacific basins south of the Tropics the eddy transport is southward and small, reflecting the dominance of the narrow southward eddy flux in the Agulhas Current and EAC. This subtropical eddy heat flow is greater than observed in lower-resolution studies (Jayne and Marotzke 2002; McCann et al. 1994; Stammer 1998).

Over 20°–30°S globally (Fig. 5d), there is a southward boundary current–driven eddy transport, peaking at 0.2 PW at 25°S. Between 30° and 35°S, the EAC and Agulhas eddy transports are largely balanced by opposing offshore transports (Fig. 3), resulting in almost zero net transport. This is probably due to strong anticyclonic eddies being shed from the eastern edge of the central current jet. From 35° to 50°S, eddies play a vital role in global ocean heat transport. In this region eddies make up over 25%–100% of the total southward heat transport. Near 40°S, the sum of the mean transports is negligible and eddies accomplish the entire southward heat transport (0.4 PW). This transport is almost 2 times what is described by either McCann et al. (1994) or Stammer (1998), and is similar in magnitude to Jayne and Marotzke's (2001) analysis. This heat transport is achieved largely by the Agulhas Retroflection and Indian Ocean sector of the SAF, as observed by Gille (2003), although a significant amount (0.1 PW) is achieved by the Brazil–Malvinas confluence. It is worth noting that much of the eddy activity in the Southern Ocean, particularly the Indian sector, is centered on the zero mass transport contour line (Fig. 1), but most of the property transport is north of this point. South of 55°S there is almost no eddy heat transport, even around Drake Passage, and the meridional heat transport is achieved by the horizontal, or gyre, mean flow. This may be caused by an Eulerian approach due to the generally cold (warm) northward (southward) mean

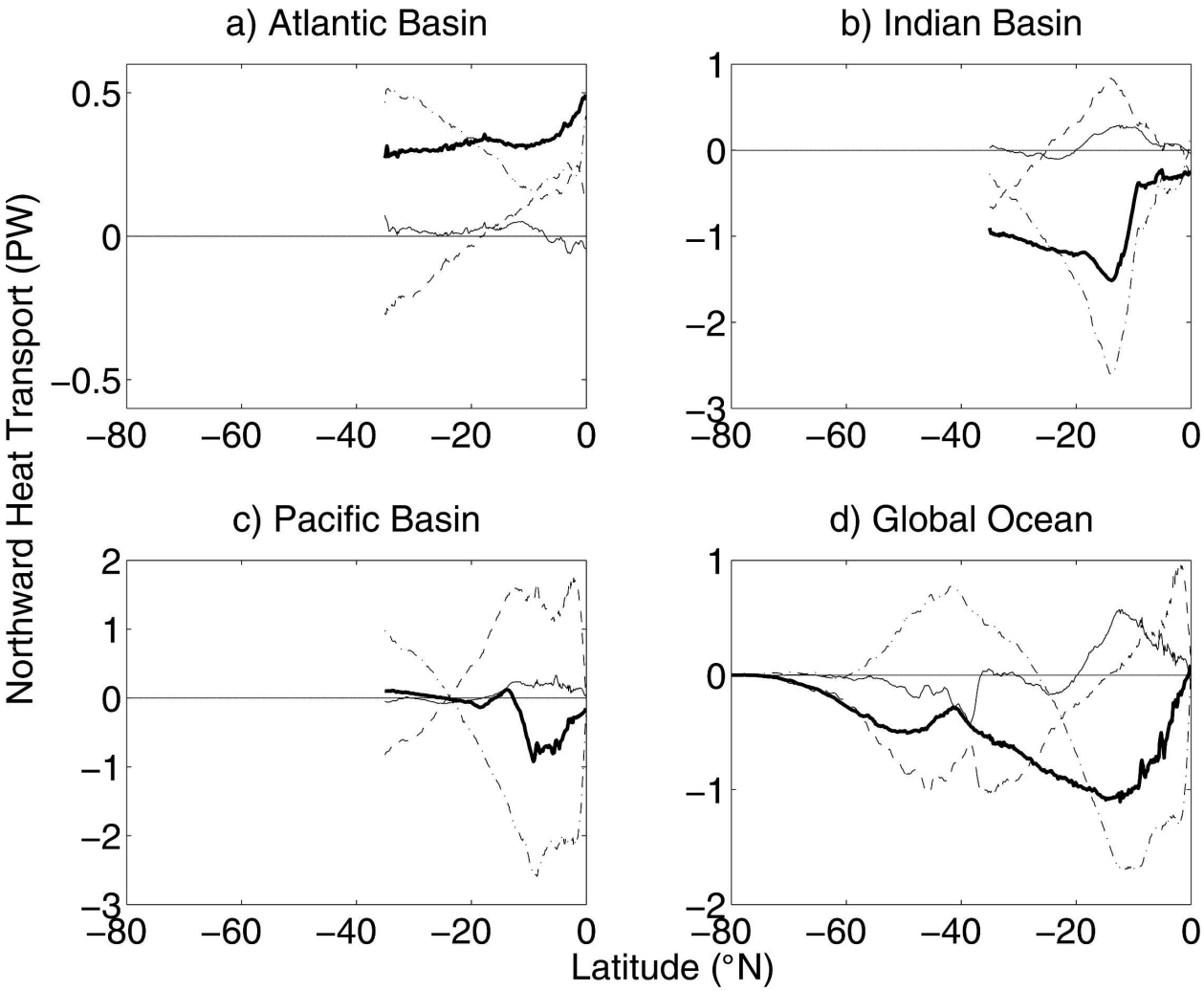


FIG. 5. Meridional total (thick), mean horizontal (dashed), mean vertical (dashed–dotted), and eddy (thin) heat transports for the (a) Atlantic, (b) Indian, (c) Pacific, and (d) global ocean basins (PW). Negative values indicate southward heat transport.

transport of the ACC when viewed across lines of constant latitude. To reduce the contribution of the horizontal gyre component, we examine the total heat transport across lines of constant mass transport (Fig. 6). This frame of reference produces a significant southward eddy heat transport of between 0.1 and 0.2 PW across the entire ACC. This is most important in the southern ACC (south of the 100-Sv line or approximately 55°S) where the eddy component transports between 30% and 100% of the total southward heat transport. The mean transport remains significant over much of the ACC however, particularly north of the 90-Sv streamline. The net northward heat transport in sections of the ACC is counterintuitive and can be explained by the greater heat gain experienced by water following the northern meanders of the ACC (Fig. 7). These streamlines travel significantly farther north than the more southerly ones and experience a large heat gain north of the polar front, as may be expected in a model with restoring boundary conditions (Karsten and Marshall 2002). This heat flux is also apparent in the Eulerian framework in the change of slope of the total heat transport across this latitude range (Fig. 5d). The convergence of the streamlines to the east results in a similar southward heat transport across northern and southern streamlines. This means that when the heat transport is summed along the streamlines bounded by Drake Passage, the net meridional heat transport of the ACC can be equatorward.

### *b. Eddy heat transport by depth*

The zonally integrated eddy transport is plotted by depth in Fig. 8. Below 2900 m the eddy transport is very small (less than 0.03 PW) and there is little eddy heat

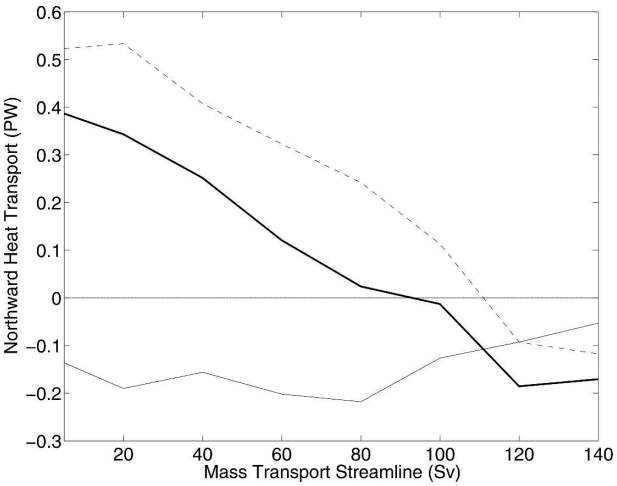


FIG. 6. Meridional heat transport integrated along Drake Passage mass transport streamlines for the total (thick), mean (dashed), and eddy (thin) components (PW). Negative values indicate southward transport.

exchange with the upper part of the ocean. This is similar to Jayne and Marotzke's (2002) value of <0.02 PW and is a small fraction (<10%) of the mean heat transport in this depth range.

Between 2900 and 900 m the eddy heat transport carries a substantially greater amount of heat than in the deep ocean. About 0.03 PW is transported poleward south of 37°S, with almost 0.08 PW equatorward north of this region of divergence. These values are similar to Jayne and Marotzke's (2002) figures south of 40°S (0.05 PW), but are larger by a factor of 5 north of this point. These results indicate that eddy heat transport is significant (over 50% of the magnitude) relative to the mean heat transport over the middepths north of 37°S, although the total heat transport itself is still very small (around 0.1 PW southward).

Heat transport over the 400–900-m depth range remains in the same direction as the deeper layers, and the region of divergence at 38°S forms the northern edge of the strong SAF-associated downwelling. Around 0.2 PW of this downwelling is circulated poleward and outcrops south of 38°S, resulting in a 0.1-PW southward heat transport in the 400–900-m layer over 36°–45°S.

Eddy heat transport is most significant in the upper ocean (<1000 m), and surface intensification of heat transport results in 50%–75% of the total eddy heat transport being achieved in the upper 400 m. Between 0° and 15°S and south of the SAF-related divergence, the zonally integrated eddy heat transport is coherent over the whole ocean depth; to the south in the sub-Antarctic latitudes, and to the north near the equator. In the subtropics, however, the eddy heat transport is not in the same direction over all depths, and carries over 0.15 PW to the north below 400 m, and over 0.2 PW to the south above this. This upper-layer eddy transport moves south in a narrow surface band, subducting to around 1000 m at the SAF with a weaker return flow between at 1500 m, circulating around 0.1 PW. Possible reasons for this difference in flow direction in the subtropics are given in section 6.

### c. Ocean to atmosphere heat flux

The zonal integral of the ocean to atmosphere heat flux, the divergence of the depth-integrated meridional heat transport, is attributed to individual basins in Fig. 9. This forms a three-term balance where the total depth-integrated divergence can be described as the sum of the (generally compensating) divergence of the mean flux and the divergence of the eddy flux. The total divergence of this depth-integrated heat flux can be interpreted as the ocean to atmosphere heat flux. The direction of the divergence agrees remarkably well with those presented by McCann et al. (1994) and Stammer et al. (2003), although the magnitude here is generally smaller. A strong anticorrelation exists between the mean and eddy divergence heat fluxes, particularly in the Tropics and around the Indian Ocean SAF, and

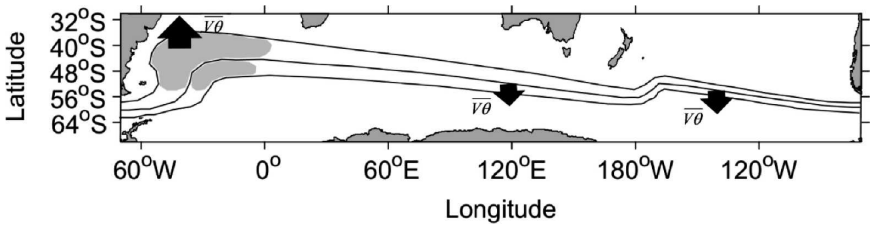


FIG. 7. Schematic diagram demonstrating heat transport $\overline{V\theta}$ (arrows) across Drake Passage mass transport streamlines. The shaded areas indicate approximate regions of heat flux into the ocean. The northernmost streamlines experience a greater heat gain and consequently have a greater northward heat transport than more southerly streamlines. To the east, the southward transports are similar for all streamlines because of their convergence; hence, the northern lines may have a net northward heat transport across them.

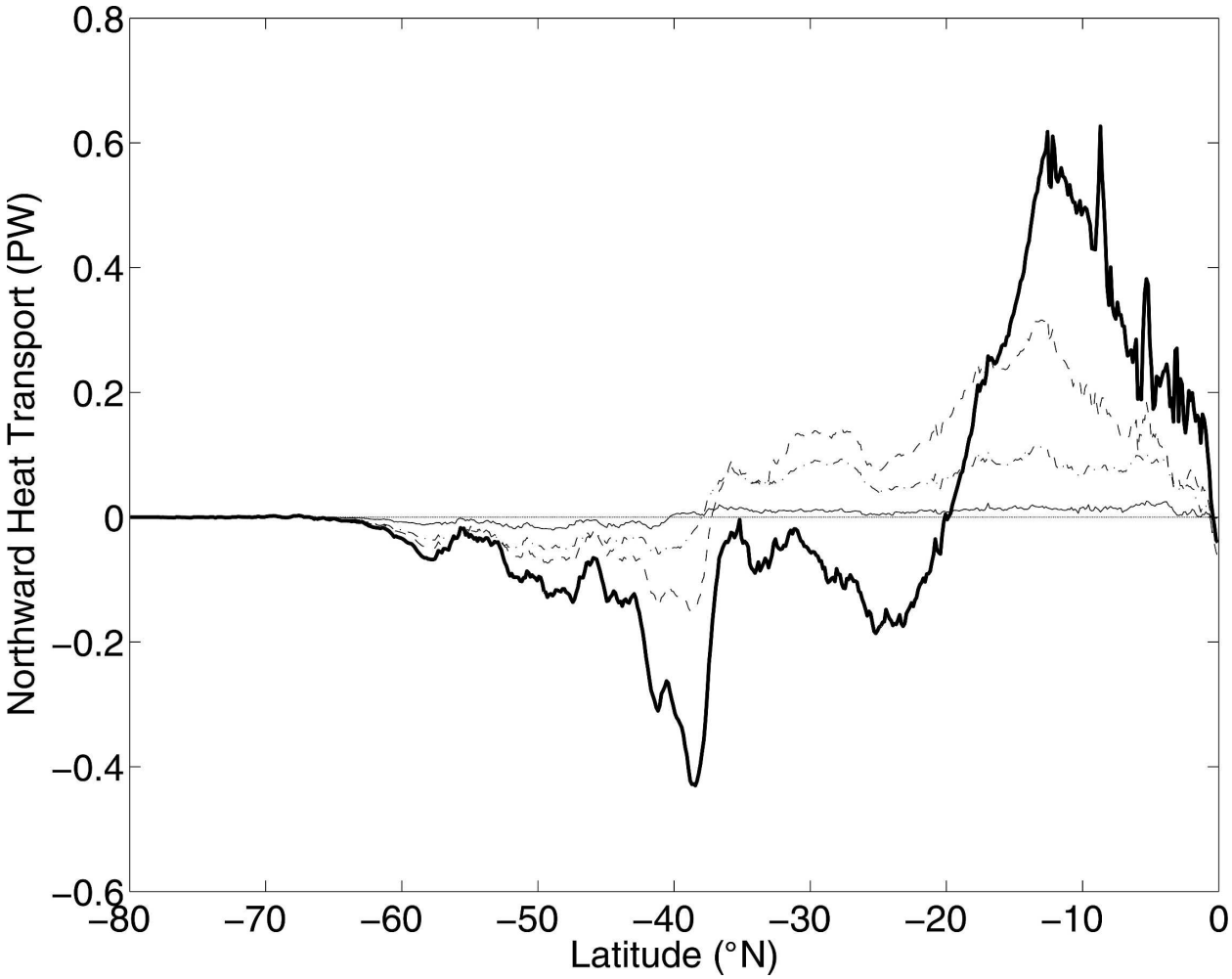


FIG. 8. Meridional northward eddy heat transport from the ocean floor to 2900 m (thin), 900 m (dashed–dotted), 400 m (dashed), and the surface (thick) (PW). Positive slopes indicate a net heat flux downward into the ocean below.

they have similar magnitudes over much of the global ocean, although the mean flux is generally slightly greater. This near equipartitioning of the total heat flux divergence contrasts with the meridional heat transport where the eddy component is generally small relative to the mean component (Fig. 5). In regions where the eddy and mean divergences have the same sign, they are out of phase with each other such that one increases while the other decreases; this is evident in the subtropical Indian basin (Fig. 9b).

The eddy heat flux divergence is greatest in the Indian Ocean, especially around the Agulhas Retroflection and SAF, where it has a high spatial frequency and large magnitudes (>200 W $m^{-2}$). The large Atlantic heat fluxes (0.2 PW) in Fig. 7a near 37°S originate almost entirely in the western Agulhas Retroflection, with a relatively small (<0.04 PW) contribution made by the Brazil–Malvinas confluence. The remainder of the Atlantic is relatively quiescent, although there is a small oceanic net heat gain over the basin, in contrast to the Indian and Pacific. The Southern Ocean poleward of 55°S and the Pacific subtropical gyre also have eddy heat fluxes close to zero, with the small-scale variability in the Pacific south of 25°S being largely due to the EAC and activity around Campbell Plateau (Fig. 9c).

In all basins south of 15°S there is a strong positive mean flux, notably in the Indian Ocean, balanced by a slightly smaller eddy flux divergence. The greater strength of this system in the Indian Ocean probably reflects heat imported from the ITF.

The compensating nature of the mean and eddy heat divergences is most apparent in regions previously identified as areas of important eddy activity. This anticorrelation between mean and eddy divergences is illustrated by the pointwise scatterplots of regional eddy and mean heat flux divergences (Fig. 10). Although the

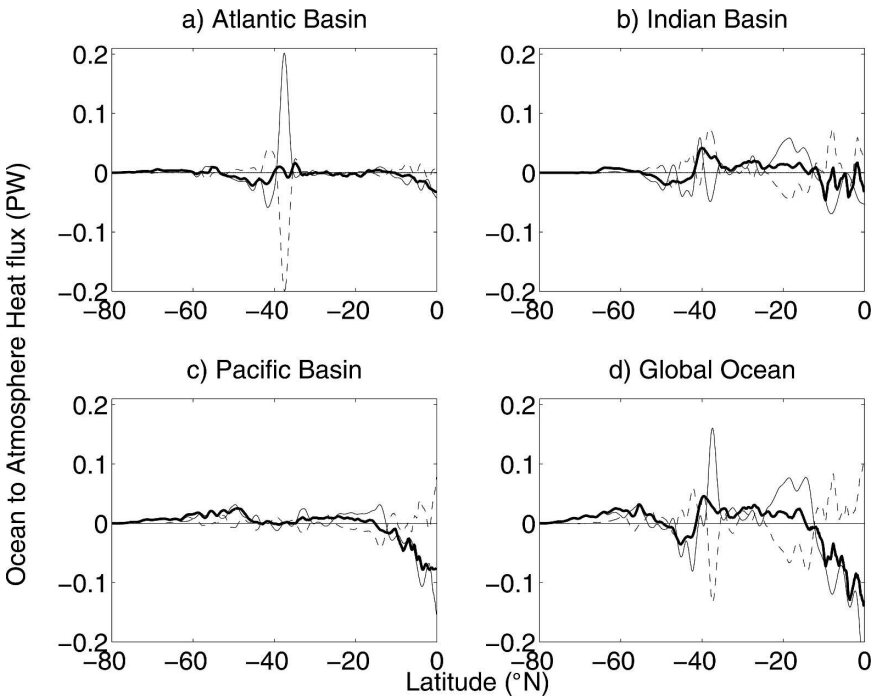


FIG. 9. Zonally integrated total (thick), mean (thin), and eddy (dashed) heat convergence (PW) for the (a) Atlantic, (b) Indian, (c) Pacific, and (d) global oceans. Positive values indicate a heat convergence.

mean and eddy fluxes are extremely large, they almost entirely offset each other, and only deviations from the 1:1 line reflect the actual local ocean to atmosphere heat flux. The tropical and boundary current regions have relatively narrower distributions around the diagonal axis and greater magnitudes than in regions of low eddy activity such as the Southern Ocean and subtropical gyres. The longer tails of the boundary current examples are much less dense than in the tropical regions, reflecting the energetic small spatial scale mesoscale eddies characteristics of the fast-flowing boundary currents. Another interesting feature of the boundary currents is the existence of large eddy divergence when there is little or no mean convergence. In these southward-flowing warm currents (the Agulhas and EAC) this may represent the stable core of the current with no net mean convergence, where eddies act to diverge heat away from the central jet. The implications and rationalization of the mean–eddy flux relationship are discussed further in section 6.

## 5. Eddy freshwater transport

### *a. Horizontal eddy freshwater transport*

The regions of vertically integrated meridional eddy freshwater divergence are shown in Fig. 11. The principal regions of importance are similar to those of the heat transport: the boundary currents, Agulhas Retroflection, and the SAF in the south Indian Ocean. It is interesting to note that these eddies largely act in the opposite direction to the heat transport and extend farther south of the SAF. Again eddy transports in the boundary currents ($>3 \times 10^{-7}$ Sv m$^{-1}$) are much greater than the ocean gyres ($<0.5 \times 10^{-7}$ Sv m$^{-1}$). Stammer's (1998) TOPEX/Poseidon eddy analysis notes the same regions of importance, with similar transport of the order of $1 \times 10^{-6}$ Sv m$^{-1}$ in the Agulhas Retroflection.

The meridional freshwater transport is attributed to individual basins in Fig. 12. South of 50°S the eddy transports are relatively small and spatially variable, resulting in almost no net eddy freshwater transport. At lower latitudes the gyre eddy transports are more spatially uniform, particularly in the Indian Ocean north of 30°S and the Pacific north of 20°S.

Eddy transport in the subtropical Atlantic makes up only 15% of the net basin northward transport and is close to zero, as was noted by McCann et al. (1994) and Stammer (1998), and in this study, for the heat transport case. The Indian and Pacific Oceans (Figs. 12b and 12c) also have significant large-scale eddy transports. Poleward of 10°S there is significant (0.2 Sv) southward

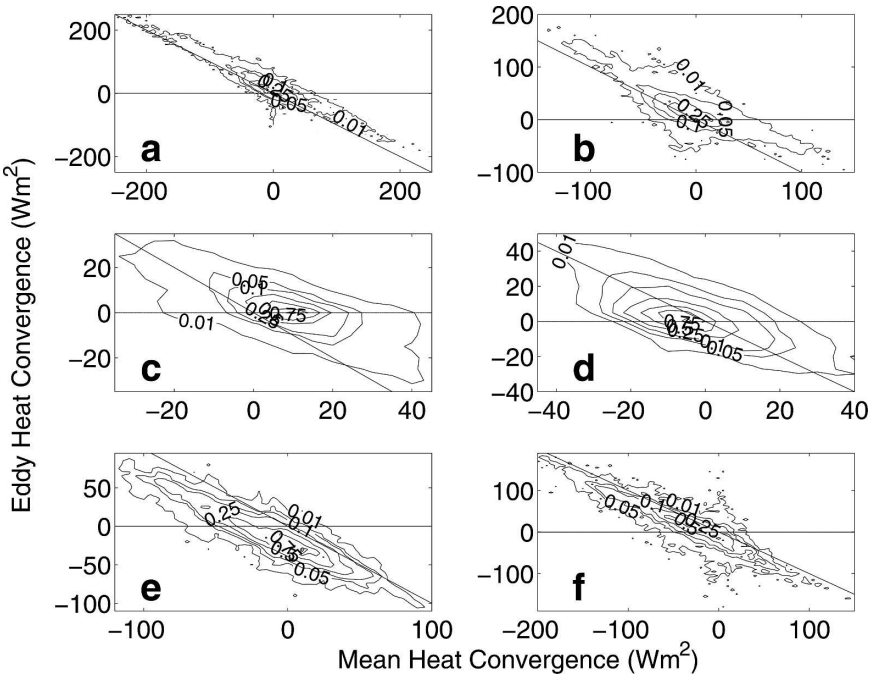


FIG. 10. Regional pointwise eddy and mean depth-integrated heat convergence correlation densities in W m$^{-2}$ for the (a) Agulhas, (b) EAC, (c) Southern Ocean, (d) southeast Pacific, (e) tropical Pacific, and (f) tropical Indian Ocean. Contours indicate the normalized number of points in a 5 × 5 W m$^{-2}$ region. Each plot contains 32000 mean and eddy flux pairs inside a 10° lat × 50° lon area. The straight line in each plot indicates a 1:1 anticorrelation.

eddy transport, peaking at 20°S, and making up 50%–100% of the total freshwater transport over these latitudes, mainly occurring in the west of the basin. Similar magnitudes of transport exist in the eastern Pacific but the peak southward transport is at 10°S. South of these peaks the eddy transports are convergent in both basins, leading to a significant net (0.2 Sv, 50% of the basins totals) freshwater convergence. This is achieved by a uniform large-scale eddy transport extending past 30°S in the Indian Ocean. In contrast, the small-magnitude finescale eddy structure seen in the Southern Ocean extends into the Pacific to 20°S, resulting in almost zero net eddy freshwater transport south of this point. The Agulhas eddies between 30° and 37°S transport about 0.025 Sv of freshwater south, but this is largely compensated for over the remainder of the basin, resulting in little overall eddy transport. A similar case exists for northward freshwater transport

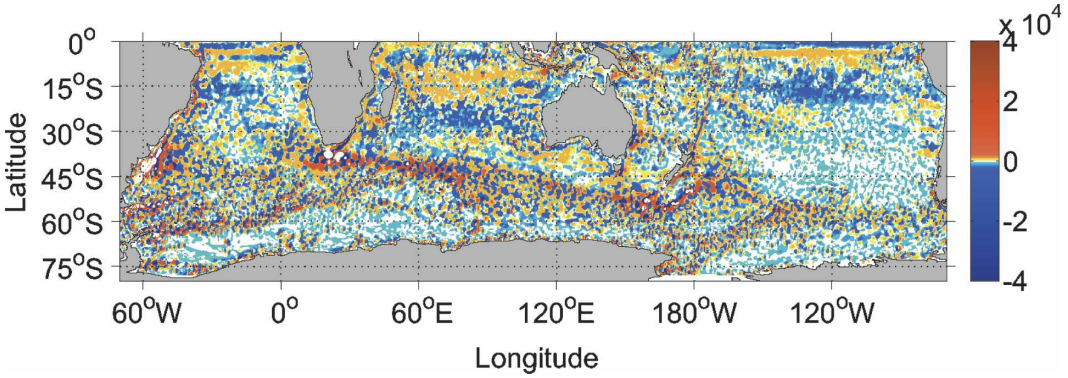


FIG. 11. Depth-integrated eddy freshwater convergence (mm yr$^{-1}$). Negative values represent freshwater di vergence. Note the compressed color scale indicating the insignificance of eddy transport across much of the ocean.

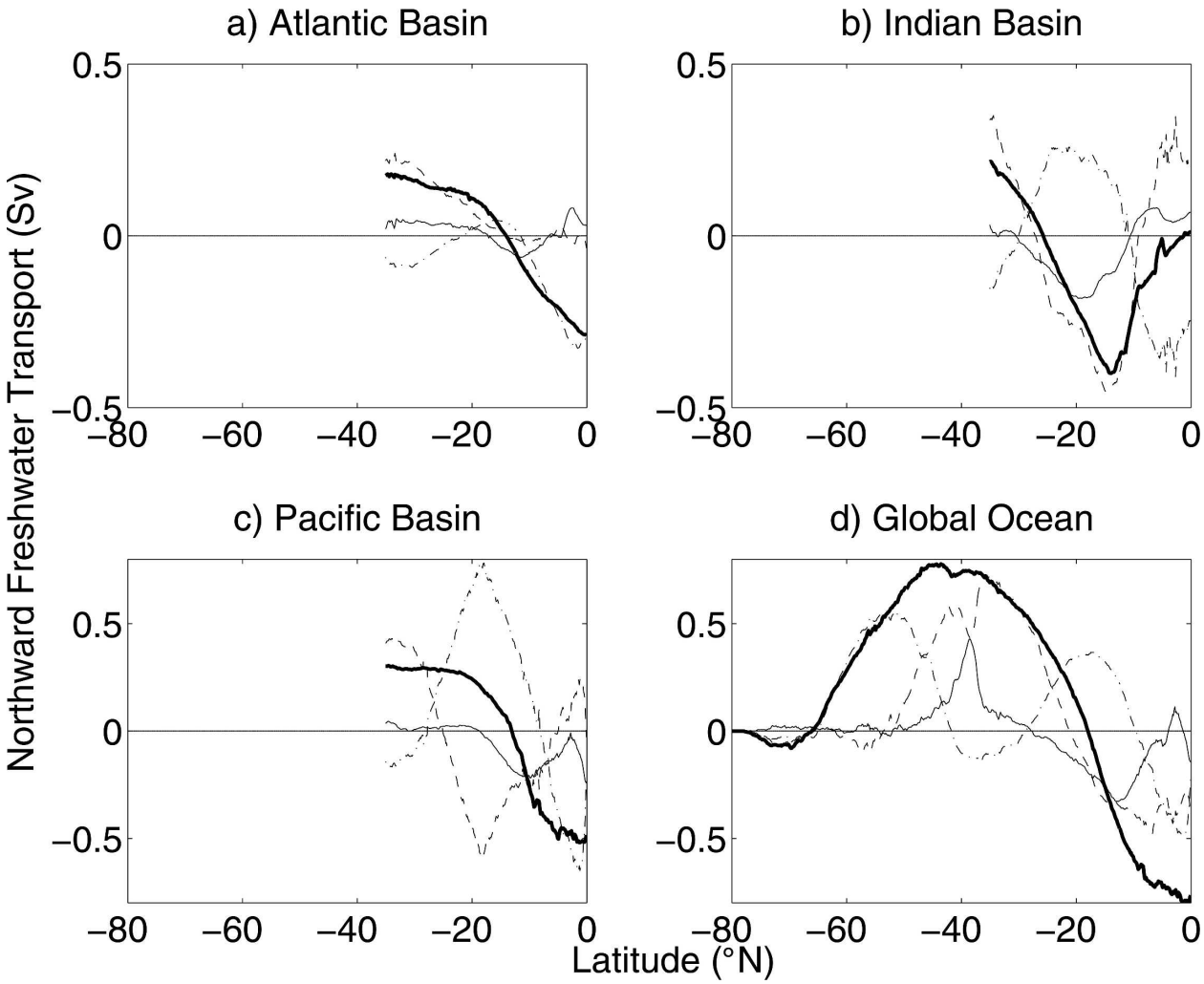


FIG. 12. Meridional total (thick), mean horizontal (dashed), mean vertical (dashed–dotted), and eddy (thin) freshwater transports for the (a) Atlantic, (b) Indian, (c) Pacific, and (d) global ocean basins (Sv). Negative values indicate southward freshwater transport.

in the EAC, although here the canceling southward transport is localized immediately to the east, rather than basin wide, as was also seen for the eddy heat transport.

The global freshwater eddy transport shows similar regions of eddy importance to the heat transport: near 40°S and north of 20°S. The eddy freshwater transport is practically zero over the Southern Ocean from Antarctica to 50°S and the cross-ACC freshwater transport is achieved almost entirely by the vertical, or overturning, component of the mean flow. The freshwater transport can be examined in quasi-Lagrangian space by looking at the transport across mass transport streamlines passing through Drake Passage (Fig. 13). The total transport is similar in magnitude and direction to the Eulerian view, indicating a more uniform freshwater flux south of the streamlines than in the heat transport case. The eddy transport in this streamline frame is small south of the 80-Sv streamline, but rapidly increases to the north, and at the northern edge of the ACC represents over 70% of the total cross-frontal transport. This strengthening in the eddy flux occurs slightly farther north in the Eulerian frame (Fig. 12d), where it increases to over 0.4 Sv (60% of the total transport) between 38° and 45°S, primarily in the Agulhas and southeast Indian Ocean SAF. The absence of a Pacific contribution was also noted by Stammer (1998). The Agulhas illustrates the pivotal role of eddies in these western boundary current extensions on the global freshwater transport (Wijffels 2001). The results presented by Stammer (1998) and McCann et al. (1994) both exhibit significant northward eddy transports around 40°S, although the flux of McCann's ½°-resolution model is small when compared with the mean flow.

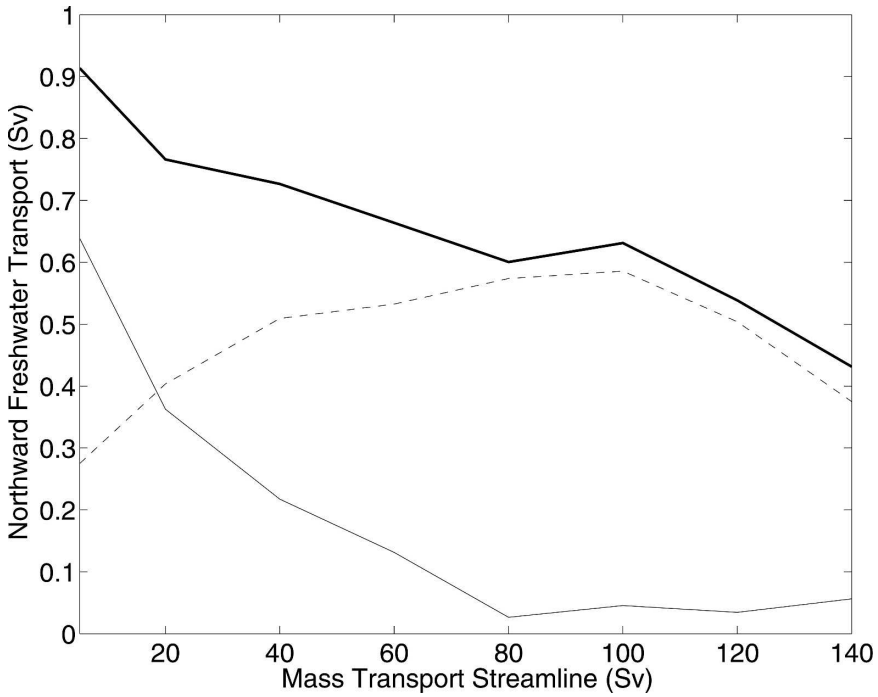


FIG. 13. Meridional freshwater transport integrated along Drake Passage mass transport streamlines for the total (thick), mean (dashed), and eddy (thin) components (Sv). Positive values indicate northward transport.

Over 20°–35°S, the eddy component is only a small fraction of the mean horizontal transport.

### b. Eddy freshwater transport by depth

The zonally integrated eddy freshwater transport is shown at selected depths in Fig. 14. The eddy component of the freshwater transport in the ocean below 2900 m or south of 50°S is very small (<0.03 Sv) and contributes little to the total transport. The strong SAF eddy transport is apparent, however, extending from 35° to 45°S and to below 900 m, and is surface intensified in the upper 400 m. On the southern side of this feature, 0.4 Sv of freshwater is subducted and transported northward. The subduction decreases with depth and at 2900 m it is effectively zero. This eddy-driven freshwater transport at the SAF sinking is central to the formation of intermediate waters between 40° and 43°S, as across these latitudes the northward eddy transport is as strong as the mean flow in the near surface (0.3 Sv northward), while the eddy-driven subduction is substantially greater (over 0.2 Sv as compared with about 0.03 Sv of mean flow; not shown here).

North of 35°S the majority of the eddy-subducted freshwater is returned to the surface although about 0.04 Sv of eddy freshwater is transported northward from 40°S to the equator in the intermediate layers below 900 m. In the upper 900 m there is a substantial southward flow increasing from zero at 30°S to almost 0.4 Sv at 15°S. This flow is in the same sense as the total freshwater transport and is of comparable size to the mean flow. The strong northward eddy freshwater

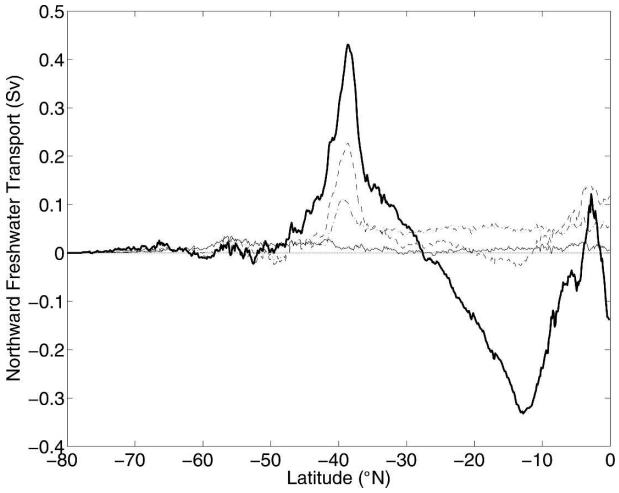


FIG. 14. Meridional northward eddy freshwater transport from the ocean floor to 2900 m (thin), 900 m (dashed–dotted), 400 m (dashed), and the surface (thick) (Sv). Positive slopes indicate a net freshwater flux into the ocean below the depth level.

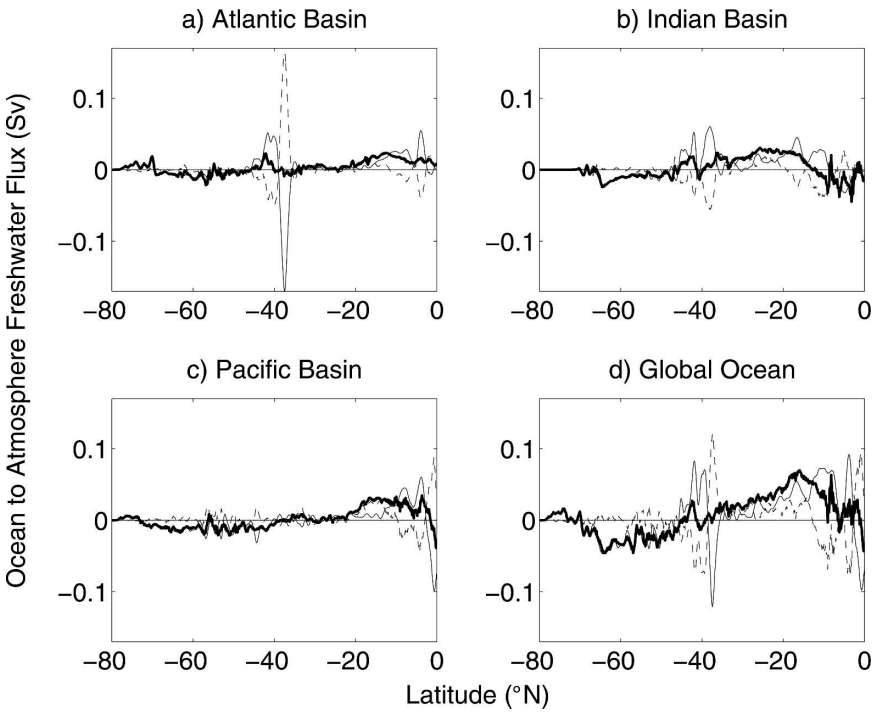


FIG. 15. Zonally integrated total (thick), mean (thin), and eddy (dashed) freshwater convergence (Sv) for the (a) Atlantic, (b) Indian, (c) Pacific, and (d) global ocean. Positive values indicate a freshwater convergence.

transport on the northern side of the 40°S SAF maximum converges with a similar southward flow from the north at around 30°S, resulting in a 0.7-Sv eddy freshwater convergence between 37° and 15°S, around 50% of the total implied surface freshwater flux.

### c. *Ocean/atmosphere eddy freshwater fluxes*

The regions of significant vertically integrated eddy freshwater divergence, zonally integrated and split by basins (Fig. 15), correspond to those areas identified as important in eddy heat transports: the Tropics, Agulhas Retroflection, and the Indian SAF. The compensatory and out-of-phase nature observed between the eddy and mean heat divergence fluxes is also seen in the freshwater divergence fluxes, although in some regions the relationship is weaker. In the Indian Ocean basin for example, the eddy flux divergence between 0° and 10°S has several narrow peaks while the mean flow exhibits only a single broad peak, and in the Pacific between 10° and 20°S where the eddy flux dominates a near-zero mean flux. This observation is supported by the mean and eddy freshwater flux pointwise correlation plots (Fig. 16) where the broader distributions in all regions indicate a weaker anticorrelation than that for the heat transport.

The Atlantic Ocean again displays a very strong (0.05–0.16 Sv) eddy divergence flux associated with the Agulhas Retroflection between 37° and 45°S (Fig. 15a). As in the heat transport case, these exchanges are balanced by larger opposing mean fluxes, and the largest peak occurs immediately south of Africa. The Indian Ocean basin (Fig. 15b) has significant eddy flux divergence from the equator to the SAF. South of this there is almost no eddy flux, although there is a significant mean freshwater flux divergence from 50°S. A strong eddy freshwater flux of over 0.05 Sv at 37°–40°S in the eastern regions of the Agulhas Retroflection acts to partially compensate the large spike discussed above, while the SAF-related divergence from 40° to 45°S acts in the same sense as in the Atlantic, resulting in a considerable (>0.06 Sv) globally integrated eddy freshwater divergence over these latitudes. In the subtropics the eddy and mean fluxes are both convergent and exist over basin-wide length scales unlike the high spatial variability in the Agulhas Retroflection or SAF. This produces a considerable total freshwater flux out of the ocean of over 0.5 Sv between 15° and 35°S.

Poleward of 20°S the Pacific basin (Fig. 15c) displays little eddy-driven freshwater flux divergence. As for heat transport, this is due to the weak, highly spatially variable fluxes seen in the Southern Ocean extending to the north, resulting in little net eddy flux when inte-

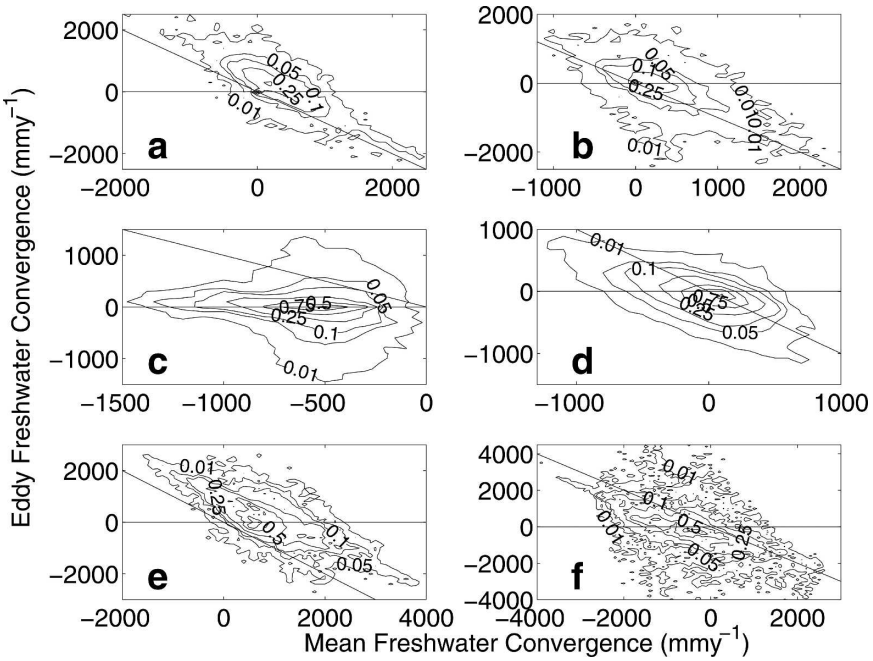


FIG. 16. Regional pointwise eddy and mean depth-integrated freshwater convergence correlation densities (mm yr$^{-1}$) for the (a) Agulhas, (b) EAC, (c) Southern Ocean, (d) southeast Pacific, (e) tropical Pacific, and (f) tropical Indian Ocean. Contours indicate the normalized number of points in a 100 × 100 mm yr$^{-1}$ region. Each plot contains 32 000 mean and eddy flux pairs inside a 10° lat × 50° lon area. The straight line in each plot indicates the 1:1 anticorrelation.

grated zonally. The small peaks present are again due to strong localized eddy divergences in the EAC and SAF around New Zealand. In contrast the mean freshwater flux divergence, particularly south of 40°S, is much less variable.

The total global freshwater flux (Fig. 15d) agrees very well with McCann et al.'s (1994) analysis, although the relative importance of the eddy flux is much greater in the 20°–50°S latitude band of this study. The eddy contribution is close to zero in the Southern Ocean from 50°S, where there is a net freshwater flux into the ocean, peaking at 65°S. Indian Ocean basin eddy flux divergences dominate the mean–eddy balance north of the Agulhas-related spike to 30°. North of this the mean flux divergence is dominant and the total flux increases to a maximum of over 0.06 Sv at 17°S.

As for heat, the freshwater regional mean eddy flux relationships (Fig. 16) show that the active eddy regions have greater magnitudes and local compensation than the Southern Ocean and gyre centers. The Southern Ocean in particular is almost symmetric around zero eddy convergence, indicating the dominance of the mean flux divergence in this region. Again the tropical areas have a more even distribution of points than the boundary currents, which have tighter central clusters of points with sparse outliers, indicating the difference in eddy horizontal scales between these regions.

## 6. Discussion and conclusions

The objective of this study was to analyze the role of mesoscale eddies in the large-scale circulation of the Southern Ocean, as modeled by the TPAC high-resolution OGCM. This analysis focused on the time-averaged ocean transport of heat and salinity over the last 11 years of the model run.

The mean volume, heat, and freshwater transports are well represented by the model, and the strengths of the western boundary currents, the ACC, and the tropical, subtropical, and polar gyres are comparable to the observations. The meridional transport exhibits strong Deacon, deep, and subtropical cells, and volume transports of water are very similar to other high-resolution model results. The ITF is present and transports around 10 Sv, 0.9 PW, and 0.2 Sv of volume, heat, and freshwater, respectively, from the Pacific to the Indian Ocean, subsequently feeding into the ACC. South of Australia there is evidence of a 9-Sv flow from the Tasman Sea into the Indian Ocean. This interbasin exchange around Australia is very significant, indicating that the Indian and Pacific Oceans should not be con-

sidered in isolation and that it may be more appropriate to examine the Indo-Pacific gyre as a whole.

This study supports the general understanding that significant eddy transports are largely restricted to small, finescale, regions of intense transport or confluence in the upper ocean. In contrast, eddy transports are negligible in comparison with the mean flow over most of the model domain, particularly in the centers of the subtropical gyres (Wunsch 1999). The poleward eddy-driven heat, and to a slightly lesser extent, freshwater, transports are extremely variable zonally and therefore circumpolar extrapolations from current meter data such as those by Phillips and Rintoul (2000) are likely to be inaccurate. Although eddies play a key role in heat transport across the northernmost edge of the ACC (De Szoeke and Levine 1981; Hall and Bryden 1982; Thompson 1993; Wunsch 1999; Rintoul et al. 2001), most of the strong eddy components occur at latitudes north of Drake Passage, and north of the 0-Sv volume transport streamline that passes through Drake Passage (cf. Fig. 1 and Figs. 3 and 11). In an Eulerian framework, the horizontal (gyre) mean circulation achieves most of the southward heat transport across the latitudes of the ACC, while the vertical (overturning) mean circulation carries freshwater north from the Southern Ocean across these latitudes. In a quasi-Lagrangian (mass transport streamline) framework, the eddy transport is very significant across the ACC, particularly for heat in its southern half, and freshwater to the north, although the mean transport remains important in both cases. The disparity between transports in these two frames of reference indicates the sensitivity of the cross-frontal transport to the coordinate system.

The regions of major Eulerian ACC eddy transport identified here occur on the northern edge of the SAF near the Agulhas Retroflection and Malvinas confluence, the southwestern Indian Ocean, and to a lesser extent south of Australia and New Zealand. The majority of the Southern Ocean, southeast Pacific, and Drake Passage all exhibit very little eddy activity. The western boundary currents and the Tropics of the Indian and Pacific basins are also regions of significant eddy contributions to the total transport of both heat and freshwater.

The relatively high resolution used here results in significantly greater eddy to mean transport ratios at high latitudes, and larger boundary current eddy transports than in lower-resolution studies, such as those by McCann et al. (1994) (½°) and Jayne and Marotzke (2002) (¼°). These relatively small scale features are more readily resolved at the ⅛° resolution used here and make greater contributions to the total transport. This higher-latitude resolution dependency may account for the similar eddy freshwater transports in model studies in the subtropical Indian Ocean, where large-scale processes rather than the narrow boundary currents appear to be responsible for eddy transport. This result conforms to the trend noted by Drijfhout (1994) for models of increasing resolution to record greater eddy transports, but with generally unchanged total transports. McClean and Semtner (1997) and Jia (2003) similarly observe that an increased resolution leads to greater eddy variability and contribution to the total transport at higher latitudes.

This result is supported by the strong compensation observed between the mean and eddy heat flux divergences. The almost one-to-one compensation appears strongest in the regions of greatest eddy transports: at the equator, around the SAF, and in the western boundary currents. This relationship shows that the increased eddy flux divergences resulting from increased model resolution do not result in a change in the total property flux to the atmosphere, but rather a compensating increase in mean flux divergence. Hence, there is only a small change in the overall global property budgets and transports with increasing model resolution and so the total transports observed here correlate well with observational and numerical studies, even at lower resolutions. A possible mechanism for this compensation may be that in regions with a strong baroclinic shear in the mean flow the increased baroclinic instability induces an opposing and compensating eddy transport, thus acting as a negative feedback mechanism. This finding may have implications for the parameterization of coarse-resolution climate models. The reduced compensation in freshwater divergences is possibly due to the more complex vertical structure of salinity, which changes the relative influence of the eddy transport in the upper layers when compared with at depth to a greater extent than in the case of heat.

Eddy transports are most significant in the upper ocean, and the upper 1000 m accounts for 75%–100% of the eddy heat and freshwater transport at most latitudes, while the upper 400 m frequently carries 75% of the total. North of the SAF, the intermediate depths from 900 to 2900 m also exhibit substantial heat and freshwater transports, although small in comparison with the surface-intensified layers. The disparity between the Eulerian heat and freshwater eddy transports, 100% and 60% of the total, respectively, across the SAF probably reflect the relatively shallow influence of eddies and the greater importance of the deep layers in freshwater transport.

The curious reversal of the transport at depth in the subtropics in both eddy heat and freshwater can be

explained by three possible scenarios. It may indicate that eddies in this region are not simple columns rotating around a vertical axis, but rather have a more complex structure over the water column. Another possibility is that the change in transport direction could be an artifact of the zonal integration across all basins. Alternatively, it could result from bathymetric considerations near the western boundary currents. The strong southward eddy heat transport in the narrow boundary currents is over the relatively shallow continental shelf and slope, while the broader northward transport associated with eddies shed from the central jet is in deep water and consequently has a greater influence at depth, resulting in northward transport below 400 m.

An interesting feature of the zonally integrated freshwater transport is that the change in transport direction in the subtropics is deeper (1500 m) than in the case of heat transport. The depth-integrated freshwater eddy transport appears to be more greatly associated with large length-scale variability away from the shallow continental shelves in the subtropics, and this possibly accounts for the deeper change in eddy transport direction. It is difficult to confidently explain these observations, however, as the zonal integration does not allow latitudinal effects to be clearly observed.

There is considerable scope for future work with the TPAC OGCM. Greater use of quasi-Lagrangian or transformed Eulerian mean (TEM) methods to describe eddy fluxes may give more insight into the cross-frontal transports. In addition, the results of this analysis lend themselves to continuing research on the influence of model resolution on eddy transports. It would be especially interesting to examine the extent to which the increased resolution–eddy transport relationship holds as models become progressively more powerful and resolve eddies on smaller and smaller scales.

*Acknowledgments.* This work was supported by the Australian government's Cooperative Research Centres Programme through the Antarctic Climate and Ecosystems Cooperative Research Center (ACE CRC). We thank T. J. McDougall and S. R. Rintoul and two anonymous reviewers for helpful comments on earlier versions of the manuscript. We also acknowledge Carl Wunsch's wonderful contribution to oceanography on the occasion of his 65th birthday.

## REFERENCES

Beckmann, A., C. W. Boning, C. Köberle, and J. Willebrand, 1994: Effects of increased horizontal resolution in a simulation of the North Atlantic Ocean. *J. Phys. Oceanogr.,* **24,** 326–344.

Biastoch, A., and W. Krauss, 1999: The role of mesoscale eddies in the source regions of the Agulhas Current. *J. Phys. Oceanogr.,* **29,** 2303–2317.

Bindoff, N. L., M. A. Rosenberg, and M. J. Warner, 2000: On the circulation and water masses over the Antarctic continental slope and rise between 80 and 150 E. *Deep-Sea Res.,* **47,** 2299–2326.

Bryan, K., 1986: Poleward buoyancy transport in the ocean and mesoscale eddies. *J. Phys. Oceanogr.,* **16,** 927–933.

De Szoeke, R. A., and M. D. Levine, 1981: The advective flux of heat by mean geostrophic motions in the Southern Ocean. *Deep-Sea Res.,* **28,** 1057–1085.

Döös, K., and D. J. Webb, 1994: The Deacon cell and the other meridional cells of the Southern Ocean. *J. Phys. Oceanogr.,* **24,** 429–442.

——, and A. Coward, 1997: The Southern Ocean as the major upwelling zone of North Atlantic Deep Water. *International WOCE Newsletter,* Vol. 27, Southampton Oceanography Center, Southampton, United Kingdom, 3–4.

Drijfhout, S. S., 1994: Heat transport by mesoscale eddies in an ocean circulation model. *J. Phys. Oceanogr.,* **24,** 353–369.

Ganachaud, A., 2003: Large-scale mass transports, water mass formation, and diffusivities estimated from World Ocean Circulation Experiment (WOCE) hydrographic data. *J. Geophys. Res.,* **108,** 3213, doi:10.1029/2002JC001565.

——, and C. Wunsch, 2000: Improved estimates of global ocean circulation, heat transport and mixing from hydrographic data. *Nature,* **408,** 453–456.

——, and ——, 2003: Large-scale ocean heat and freshwater transports during the World Ocean Circulation Experiment. *J. Climate,* **16,** 696–705.

Gent, P. R., and J. C. McWilliams, 1990: Isopycnal mixing in ocean circulation models. *J. Phys. Oceanogr.,* **20,** 150–155.

Gille, S. T., 2003: Float observations of the Southern Ocean. Part II: Eddy fluxes. *J. Phys. Oceanogr.,* **33,** 1182–1196.

Gordon, A. L., 2001: Interocean exchange. *Ocean Circulation and Climate: Observing and Modelling the Global Ocean,* G. Siedler, J. Church, and J. Gould, Eds., Academic Press, 303–314.

——, J. B. Weiss, W. M. Smethie, and M. J. Warner, 1992: Thermocline and intermediate water communication between the South Atlantic and Indian Oceans. *J. Geophys. Res.,* **97,** 7223–7249.

Gouretski, V. V., and K. Janke, 1998: A new world ocean climatology: Optimal interpolation of historical and WOCE hydrographic data on neutral surfaces. WOCE Tech. Rep. 162/89, WHP Special Analysis Centre, 40 pp.

Hall, M. M., and H. L. Bryden, 1982: Direct estimates and mechanisms of ocean heat transport. *Deep-Sea Res.,* **29,** 339–359.

Jayne, S. R., and J. Marotzke, 2001: The dynamics of ocean heat transport variability. *Rev. Geophys.,* **39,** 385–411.

——, and ——, 2002: The oceanic eddy heat transport. *J. Phys. Oceanogr.,* **32,** 3328–3345.

Jia, Y., 2003: Ocean heat transport and its relationship to ocean circulation in the CMIP coupled models. *Climate Dyn.,* **20,** 153–174.

Kalnay, E., and Coauthors, 1996: The NECP/NCAR 40-Year Reanalysis Project. *Bull. Amer. Meteor. Soc.,* **77,** 437–471.

Karoly, D. J., P. C. McIntosh, P. Berrisford, T. J. McDougall, and A. C. Hirst, 1997: Similarities of the Deacon cell in the Southern Ocean and Ferrel cells in the atmosphere. *Quart. J. Roy. Meteor. Soc.,* **123,** 519–526.

Karsten, R. H., and J. Marshall, 2002: Constructing the residual

circulation of the ACC from observations. *J. Phys. Oceanogr.,* **32,** 3315–3327.

Levitus, S., 1982: *Climatological Atlas of the World Ocean.* NOAA Prof. Paper 13, 173 pp. and 17 microfiche.

Maamaatuaiahutapu, K., V. Garcon, C. Provost, and H. Mercier, 1998: Transports of the Brazil and Malvinas Currents at their confluence. *J. Mar. Res.,* **56,** 417–438.

Marshall, D., 1997: Subduction of water masses in an eddying ocean. *J. Mar. Res.,* **55,** 201–222.

Marshall, J., and T. Radko, 2003: Residual-mean solutions for the Antarctic Circumpolar Current and its associated overturning circulation. *J. Phys. Oceanogr.,* **33,** 2341–2354.

Mata, M. M., M. Tomczak, S. Wijffels, and J. A. Church, 2000: East Australian Current volume transports at 30 degree S: Estimates from the World Ocean Circulation Experiment hydrographic sections PR11/P6 and the PCM3 current meter array. *J. Geophys. Res.,* **105,** 28 509–28 526.

McCann, M. P., A. J. Semtner, and R. M. Chervin, 1994: Transports and budgets of volume, heat, and salt from a global eddy-resolving ocean model. *Climate Dyn.,* **10,** 59–80.

McClean, J. L., and A. J. Semtner, 1997: Comparisons of mesoscale variability in the Semtner–Chervin 1/4 model, the Los Alamos Parallel Ocean Program 1/6 model, and TOPEX/POSEIDON data. *J. Geophys. Res.,* **102,** 25 203–25 226.

McIntosh, P. C., and T. J. McDougall, 1996: Isopycnal averaging and the residual mean circulation. *J. Phys. Oceanogr.,* **26,** 1655–1660.

Olbers, D., and M. Visbeck, 2005: A model of the zonally averaged stratification and overturning in the Southern Ocean. *J. Phys. Oceanogr.,* **35,** 1190–1205.

Phillips, H. E., and S. R. Rintoul, 2000: Eddy variability and energetics from direct current measurements in the Antarctic Circumpolar Current south of Australia. *J. Phys. Oceanogr.,* **30,** 3050–3076.

Rhines, P. B., 2001: Mesoscale eddies. *Encyclopedia of Ocean Science,* M. Steele, K. K. Turekian, and S. A. Thorpe, Eds., Academic Press, 1982–1992.

Rintoul, S. R., and S. Sokolov, 2001: Baroclinic transport variability of the Antarctic Circumpolar Current south of Australia (WOCE repeat section SR3). *J. Geophys. Res.,* **106,** 2795–2814.

——, C. W. Hughes, and D. Olbers, 2001: The Antarctic Circumpolar Current system. *Ocean Circulation and Climate: Observing and Modelling the Global Ocean,* G. Siedler, J. Church, and J. Gould, Eds., Academic Press, 271–302.

Roberts, M., and D. Marshall, 1998: Do we require adiabatic dissipation schemes in eddy-resolving ocean models? *J. Phys. Oceanogr.,* **28,** 2050–2063.

Semtner, A. J., and R. M. Chervin, 1992: Ocean general-circulation from a global eddy-resolving model. *J. Geophys. Res.,* **97,** 5493–5550.

Sloyan, B. M., and S. R. Rintoul, 2001: The Southern Ocean limb of the global deep overturning circulation. *J. Phys. Oceanogr.,* **31,** 143–173.

Smith, R. D., and P. R. Gent, 2004: Anisotropic Gent–McWilliams parameterization for ocean models. *J. Phys. Oceanogr.,* **34,** 2541–2564.

Spall, M. A., and D. C. Chapman, 1998: On the efficiency of baroclinic eddy heat transport across narrow fronts. *J. Phys. Oceanogr.,* **28,** 2275–2287.

Speich, S., P. de Vries, S. Drijfhout, K. Doos, A. Ganachaud, and R. March, 2002: Tasman leakage: A new route in the global ocean conveyor belt. *Geophys. Res. Lett.,* **29,** 551–554.

Stammer, D., 1998: On eddy characteristics, eddy transports, and mean flow properties. *J. Phys. Oceanogr.,* **28,** 727–739.

——, and Coauthors, 2003: Volume, heat, and freshwater transports of the global ocean circulation 1993–2000, estimated from a general circulation model constrained by World Ocean Circulation Experiment (WOCE) data. *J. Geophys. Res.,* **108,** 3007–3029.

Stramma, L., and J. Lutjeharms, 1997: The flow field of the subtropical gyre of the South Indian Ocean. *J. Geophys. Res.,* **102,** 5513–5530.

Thompson, S. R., 1993: Estimation of the transport of heat in the Southern Ocean using a fine-resolution numerical model. *J. Phys. Oceanogr.,* **23,** 2493–2497.

Whitworth, T., III, and R. G. Peterson, 1985: The volume transport of the Antarctic Circumpolar Current from three-year bottom pressure measurements. *J. Phys. Oceanogr.,* **15,** 810–816.

Wijffels, S., 2001: Ocean transport of fresh water. *Ocean Circulation and Climate: Observing and Modelling the Global Ocean,* G. Siedler, J. Church, and J. Gould, Eds., Academic Press, 475–488.

——, R. W. Schmitt, H. L. Bryden, and A. Stigebrandt, 1992: Transport of freshwater by the oceans. *J. Phys. Oceanogr.,* **22,** 155–162.

Willebrand, J., and D. B. Haidvogel, 2001: Numerical ocean circulation modelling: Present status and future directions. *Ocean Circulation and Climate: Observing and Modelling the Global Ocean,* G. Siedler, J. Church, and J. Gould, Eds., Academic Press, 547–556.

Wunsch, C., 1999: Where do eddy heat fluxes matter? *J. Geophys. Res.,* **104,** 13 235–13 249.

Yaremchuck, M., N. L. Bindoff, J. Schroter, D. Nechaev, and S. R. Rintoul, 2001: On the zonal and meridional circulation and ocean transports between Tasmania and Australia. *J. Geophys. Res.,* **106,** 2795–2814.